Kaon production in Au+Au collisions at 11.6*A* GeV/*c*

L. Ahle,[7,*] Y. Akiba,[5] K. Ashktorab,[1] M. D. Baker,[7,†] D. Beavis,[1] H. C. Britt,[6] J. Chang,[3] C. Chasman,[1] Z. Chen,[1,‡] C.-Y. Chi,[13] Y. Y. Chu,[1] V. Cianciolo,[7,§] B. A. Cole,[7,‖] H. J. Crawford,[2] J. B. Cumming,[1] R. Debbe,[1] J. C. Dunlop,[7] W. Eldredge,[3] J. Engelage,[2] S.-Y. Fung,[3] E. Garcia,[11] S. Gushue,[1] H. Hamagaki,[12] L. F. Hansen,[6] R. S. Hayano,[8] G. Heintzelman,[7] E. Judd,[2] J. Kang,[10] E.-J. Kim,[1,10] A. Kumagai,[9] K. Kurita,[9,¶] J.-H. Lee,[1] J. Luke,[6] Y. Miake,[9] A. Mignerey,[11] B. Moskowitz,[1] M. Moulson,[13] C. Muentz,[1,**] S. Nagamiya,[4] M. N. Namboodiri,[6] C. A. Ogilvie,[7] J. Olness,[1] L. P. Remsberg,[1] H. Sako,[8,††] T. C. Sangster,[6] R. Seto,[3] J. Shea,[11] K. Shigaki,[8,‡‡] R. Soltz,[7,*] S. G. Steadman,[7] G. S. F. Stephans,[7] M. J. Tannenbaum,[1] J. H. Thomas,[6,§§] S. Ueno-Hayashi,[9] F. Videbaek,[1] F. Wang,[13,§§] Y. Wu,[13] H. Xiang,[3] G. H. Xu,[3] K. Yagi,[9] H. Yao,[7] W. A. Zajc,[13] and F. Zhu[1]

(E-802 Collaboration)

[1]*Brookhaven National Laboratory, Upton, New York 11973*
[2]*University of California, Space Sciences Laboratory, Berkeley, California 94720*
[3]*University of California, Riverside, California 92507*
[4]*High Energy Accel. Res. Organization (KEK), Tsukuba, Ibaraki 305, Japan*
[5]*High Energy Accel. Res. Organization (KEK), Tanashi-branch, (Tanashi) Tokyo 188, Japan*
[6]*Lawrence Livermore National Laboratory, Livermore, California 94550*
[7]*Massachusetts Institute of Technology, Cambridge, Massachusetts 02139*
[8]*Department of Physics, University of Tokyo, Tokyo 113, Japan*
[9]*University of Tsukuba, Tsukuba, Ibaraki 305, Japan*
[10]*Yonsei University, Seoul 120-749, Korea*
[11]*University of Maryland, College Park, Maryland 20742*
[12]*Center for Nuclear Study, School of Science, University of Tokyo, Tanashi, Tokyo 188, Japan*
[13]*Columbia University, New York 10027 and Nevis Laboratories, Irvington, New York 10533*

(Received 12 March 1998)

A systematic study of the spectra and yields of K^+ and K^- is reported by experiment E866 as a function of centrality in Au+Au collisions at 11.6*A* GeV/*c*. The invariant transverse spectra for both kaon species are well described by exponentials in m_t, with inverse slope parameters that are largest at midrapidity and which increase with centrality. The inverse slopes of the K^+ spectra are slightly larger than the inverse slopes of the K^- spectra. The kaon rapidity density peaks at midrapidity with the K^+ distribution wider in rapidity than K^-. The integrated total yields of K^+ and K^- increase nonlinearly and steadily with the number of projectile participants. The yield per participant for kaons is two to three times larger than the yield from *N*-*N* collisions. This enhancement suggests that the majority of kaons in central Au+Au reactions are produced in secondary hadronic collisions. There is no evidence for an onset of additional kaon production from a possible small volume of baryon-rich quark-gluon plasma. The differences between K^+ and K^- rapidity distributions and transverse spectra are consistent with a lower phase space for K^- production due to a higher energy threshold. These differences also exclude simple thermal models that assume emission from a common equilibrated system. [S0556-2813(98)01011-5]

PACS number(s): 25.75.−q, 13.85.Ni, 21.65.+f

*Present address: Lawrence Livermore National Laboratory, Livermore, CA 94550.
†Present address: Brookhaven National Laboratory, Upton, NY 11973.
‡Present address: Renaissance Technologies Corp., Stony Brook, NY 11790.
§Present address: Oak Ridge National Laboratory, Oak Ridge, Tennessee 37831.
‖Present address: Columbia University and Nevis Laboratories, Irvington, NY 10533.
¶Present address: The Institute of Physical and Chemical Research (RIKEN), Saitama 351-01, Japan.
**Present address: Goethe Universitaet, Institut fuer Kernphysik, Frankfurt, Germany.
††Present address: University of Tsukuba, Tsukuba, Ibaraki 305, Japan.
‡‡Present address: Center for Nuclear Study, School of Science, Univerity of Tokyo, Tanashi, Tokyo 188, Japan.
§§Present address: Lawrence Berkeley National Laboratory, Berkeley, California 94720.

I. INTRODUCTION

The collision of two heavy ions at AGS energies is a complex process that involves the multiple collisions of hadrons, transferring energy from the initial longitudinal motion into both the production of particles and transverse motion. The very dense system formed in these collisions may reveal information on the possible existence of the baryon-rich quark-gluon plasma (QGP) [1] and/or the possible medium dependence of hadronic masses [2]. The search for such new physics requires a solid understanding of the reaction dynamics, the roles played by multiple collisions, excited resonances, and the balance between absorption and initial production of particles. This foundation is necessary because any signatures of new physics will be sitting in the dominant environment of hadronic rescattering.

Such a foundation is provided by measuring the spectra and yields of produced particles as a function of centrality of the reaction. As an example, the yield of kaons is enhanced in central $A+A$ reactions compared to A times the yield in nucleon-nucleon collisions [3]. The enhancement is possibly explained [4–6] by secondary collisions in the heavy-ion reaction, where each hadron can undergo several collisions, and each collision has a certain probability of producing a kaon. This mechanism is aided by many of the secondary collisions being between one or two hadronic resonances with the energy of the resonances available for kaon production. The role of these secondary collisions in particle production can be probed by measuring how the spectra and yield of kaons vary with centrality.

This paper reports on the systematics of kaon production in Au+Au collisions at 11.6A GeV/c. The Collaboration has also reported on particle production in $p+A$ [7] and Si $+A$ [8] reactions at AGS energies. This wide range of measurements provides a comprehensive data set of particle production at AGS energies.

From our previous studies [9], the measured proton dN/dy in Au+Au central collisions has a maximum at midrapidity, consistent with the formation of a dense, baryon-rich system. Hadronic cascade models predict that the inner region of the collision zone may reach greater than five times normal nuclear density [5,6]. Approximately one-third of the colliding matter is predicted to be in such a dense environment [6]. Experimentally it is a challenge to characterize dense hadronic matter and then to find any evidence whether such matter has been converted to a baryon-rich quark-gluon plasma.

One method is to measure the systematics of kaon production as a function of the centrality of a heavy-ion reaction. The kaon production rate from a QGP has been predicted to be larger than the hadronic production rate [10]. The more central the collision, the larger the volume of very dense matter. A small but increasing volume of QGP might be observable as an additional increase in kaon production beyond the hadronic enhancement from multiple collisions. Separating these two effects will be experimentally difficult.

There are several predictions [11] that at densities from one to three times normal nuclear density, kaons might change their properties. In these models K^- are predicted to interact attractively with baryons. In nuclear matter, these interactions can be implicitly accounted for by either an attractive mean-field [12,13] or by decreasing the K^- effective mass with density [11]. Experiments with kaonic atoms [14] confirm the existence of an attractive K^- nuclear potential but do not provide detailed information on its strength. These same models predict that K^+ have a repulsive interaction with baryons [12,13]. In heavy-ion reactions, these models suggest that the spectra of K^+ and K^- may be shifted in opposite directions [15,12], pushing the K^+ to higher transverse momentum and pulling the K^- to lower values of transverse momentum. The measured K^+ and K^- spectra as a function of centrality provide a test for the predicted in-medium properties of kaons.

The following section describes experiment E866 at the AGS and the methods used to analyze the data. Section III contains the experimental results, the invariant transverse spectra of K^+ and K^- as a function of centrality, the rapidity density and the inverse slope distributions as a function of centrality, and the integrated yields of kaons per event. In Sec. IV the differences between K^+ and K^- emission are discussed. The $K\pi$ ratios measured in Au+Au are compared to results from previous AGS measurements in Sec. V. The conclusions are presented in Sec. VI.

II. EXPERIMENT AND DATA ANALYSIS

The E866 experiment at the AGS measured Au+Au reactions at 11.6A GeV/c in the fall of 1994. The apparatus [9,16] consists of event-characterizing global detectors and two magnetic spectrometers as is shown in Fig. 1.

The Au beam impinged on a Au foil 975 mg/cm^2 thick; a thickness that provides approximately a 2% interaction probability. The intensity of the Au beam was kept less than 1×10^5 particles per spill, for a spill duration of 1 s.

A set of counters upstream of the target defined a ''good'' beam particle. The charge (Z) and time of arrival of the beam particle were measured with a quartz Cerenkov radiator. Beam pile-up was rejected if two beam nuclei were within 0.5μs and by a tight gate on $Z=79\pm3$ on this counter. A counter with a 1 cm diameter hole 1 m upstream of the target rejected beam halo.

Downstream of the target (10.6 m) was a ''bullseye'' quartz Cerenkov radiator [17] viewed by eight photomultiplier tubes. This provided an interaction trigger by rejecting events with a bullseye signal $Z>74$. A software cut was applied off-line that tightened the interaction trigger to reject events with $Z>68$. The events selected by the interaction trigger and software cut had a cross section of 5.1 b. This is lower than the full interaction cross section of 6.8 b because the most peripheral reactions are not selected by the trigger. Target-out runs were used to determine the background contribution to the interaction cross section and to the spectra in the spectrometers. The target-out contribution to kaon spectra was negligible.

The two spectrometers of E866 can independently rotate. The spectrometer Henry Higgins (also used in E802 and E859) has a 25 msr solid angle, with $\Delta\theta\sim14°$. By rotating the spectrometer, the acceptance covers lab angles from 14°–58°. The Forward spectrometer commissioned for E866 has a 6 msr solid angle, with $\Delta\theta\sim4°$, and by rotation covers lab angles of 6°–28°. The acceptances for kaons in these devices are shown in Fig. 2. Data were collected with

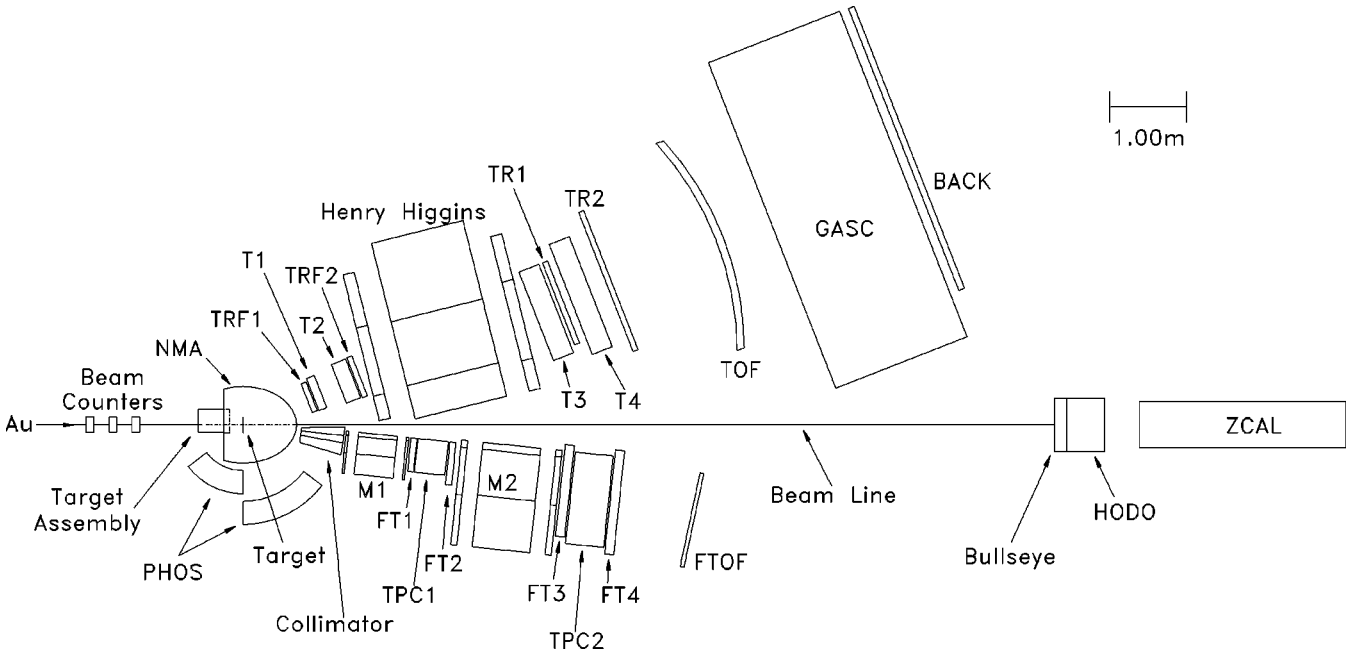

FIG. 1. The experimental layout of E866 in the Fall of 1994 showing the multiplicity array (NMA), the zero-degree calorimeter (ZCAL), the interaction trigger (Bullseye), and the Henry Higgins spectrometer consisting of drift chambers (T1-T4), wire chambers (TRF1,2 and TR1,2), a time-of-flight wall (TOF) and a gas-Cerenkov detector (GASC). The forward spectrometer consists of a sweeping magnet (M1), analyzing magnet (M2), drift chambers (FT1-4), two time projection chambers (TPC1,2) and a time-of-flight wall (FTOF). A scintillator array (PHOS) for particle spectra at back-angles and a hodoscope (HODO) of crossed XY slats complete the detector hardware of E866.

both polarity settings of the dipole magnets, equalizing the acceptance for oppositely charged particles.

Both spectrometers have tracking systems before and after a dipole magnet. The Henry Higgins spectrometer uses a combination of drift and multiwire chambers to locate the tracks, whereas the Forward spectrometer uses tracking stations consisting of a time-projection chamber (TPC) sandwiched by drift chambers. The TPC data are used for the tracking pattern recognition in the high occupancy environment and the data from the drift chambers improve the momentum resolution.

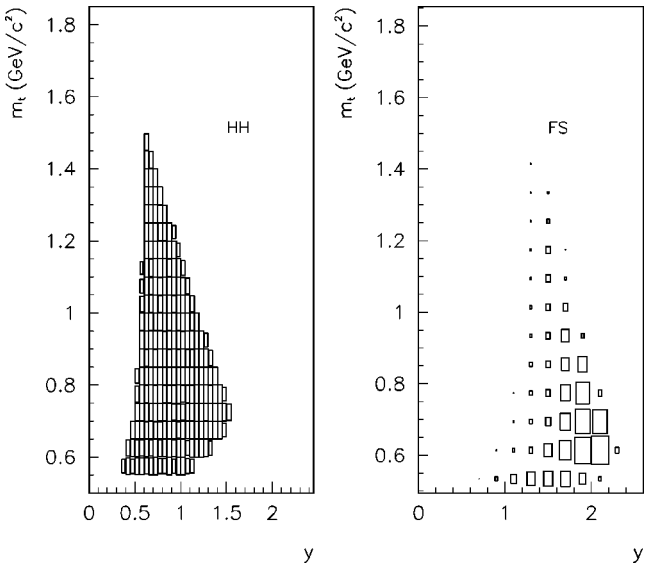

FIG. 2. The acceptance for kaons in the Henry Higgins spectrometer (left panel) and in the Forward spectrometer (right panel). For the Henry Higgins the area of the boxes indicate the relative acceptance of each bin, while for the Forward spectrometer the boxes represent the number of measured kaons over all the angle settings.

The experiment was primarily triggered by spectrometer-based triggers. For the Forward spectrometer, the trigger used the FT2 and FT3 drift chambers (Fig. 1) located before and after the momentum analyzing magnet ($M2$). The trigger was defined as FT2$\cap$FT3, where these symbols represent any hits in one of the first two planes of FT2 (FT3) chambers. For the Henry Higgins spectrometer the trigger was a coincidence between any hit in a multiwire chamber (TR1 in Fig. 1) behind the magnet and any hit in the time-of-flight (TOF) wall. The Henry Higgins spectrometer had the additional feature of an online particle identification trigger (LVL2) [18]. The trigger looped over combinations of hits in the TOF wall and two multiwire chambers (TR1 and TR2) behind the magnet. A CAMAC-based series of lookup tables was used to veto events that did not have a track consistent with a kaon mass. Events were not vetoed if they contained a high-momentum track ($p>1.7$ GeV/c) where the online particle identification may be ambiguous. The LVL2 trigger enhanced the fraction of events with kaons on tape. The inefficiency of this trigger was measured to be less than 1 %.

Both spectrometers have a segmented TOF wall of vertical scintillator slats. Each slat is instrumented with photomultiplier tubes at each end. The measured resolutions of the Henry Higgins and Forward spectrometer TOF walls are $\sigma=130$ ps, and $\sigma=75$ ps respectively. The momentum range for identified kaons is $0.3<p<1.74$ GeV/c and $0.5<p<3.0$ GeV/c for the Henry Higgins and Forward spectrometer, respectively.

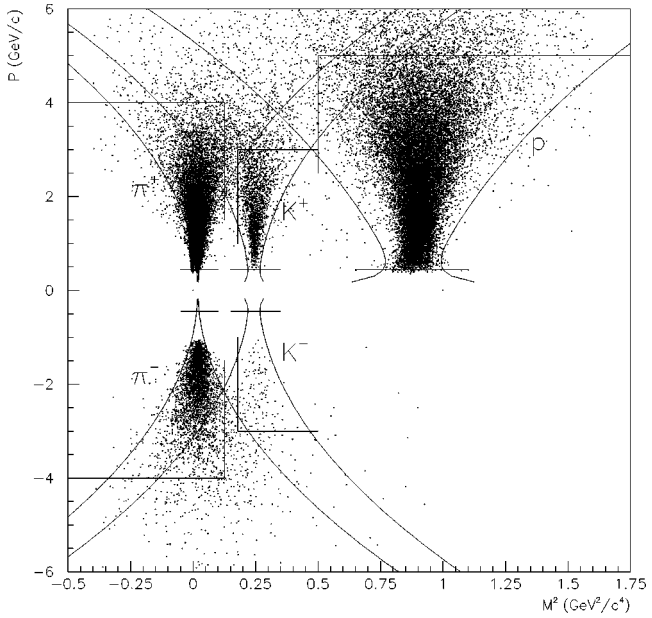

FIG. 3. A scatter plot of M^2 versus p in a typical forward spectrometer run at the 14° spectrometer setting. The curves in the figures are PID boundaries set at $\pm 2.5\sigma_{M^2}$ from the nominal mass of the particle. The additional lines are further cuts made to minimize contamination.

The particle identification in the Forward spectrometer was provided by 100 slats of time-of-flight (FTOF) counters located 6 m from the target. Mass square (M^2) of a particle is calculated from its momentum p, time-of-flight t, and path length L as $M^2=p^2[(ct/L)^2-1]$. Particle identification cuts were applied in M^2 versus p space. Figure 3 shows a scatter plot of M^2 versus p in a typical run at 14° spectrometer setting. Pions, kaons, and (anti)protons are well separated. The curves in the figures are PID boundaries set at $\pm 2.5\sigma_{M^2}$ from the nominal mass of the particle. In addition, the following cuts were made to suppress contamination from other particles: $M^2<0.125$ GeV$^2/c^4$ and $p<4$ GeV/c for $\pi^{\pm}$, $M^2>0.18$ GeV$^2/c^4$ and $p<3$ GeV/c for $K^{\pm}$, $M^2>0.50$ GeV$^2/c^4$ and $p<5$ GeV/c for p. These cuts are also indicated in the figure. The remaining pion and proton contamination in kaon sample was estimated by a multi-Gaussian fit to the M^2 distribution in momentum slices and was subtracted from the data.

For the Henry Higgins spectrometer, particle identification cuts were made in $1/\beta$ versus momentum space at a $\pm 3\sigma$ level (Fig. 4), where β is the velocity of particles as determined by the TOF wall. The backgrounds to both the K^+ and K^- samples were less than 2% within the momentum range used ($0.3<p<1.74$ GeV/c).

E866 has two detectors that measured the global characteristics of each event, a multiplicity array (NMA) and a Fe-scintillator sandwich type calorimeter (ZCAL) with an 1.5° opening angle around the beam axis. The multiplicity array was not used in this analysis. The energy deposited into the calorimeter (E_{ZCAL}) for interaction events after target-out subtraction is shown in Fig. 5. The boundaries of the five centrality event classes used in the analysis, discussed later, are also indicated in the figure. The calorimeter was calibrated to maintain the fragmented-beam peak at the kinetic

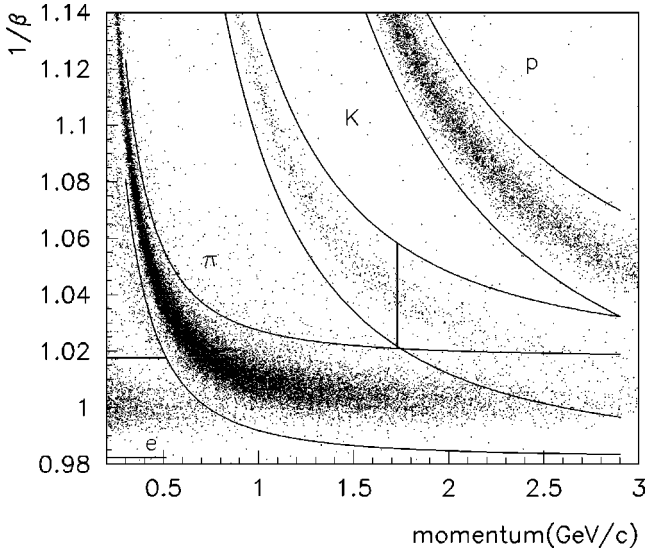

FIG. 4. A scatter plot of $1/\beta$ versus p for the Henry Higgins spectrometer. The particle identification bands are at $\pm 3\sigma$ in the measured $1/\beta$.

energy of the beam $E^{\mathrm{kin}}_{\mathrm{beam}}=2123$ GeV. Fragmented-beam events are those that react just upstream of the calorimeter. This calibration was performed for each run to compensate for the radiation-damage decrease in calorimeter light output. The decrease in light output over the entire 1994 running period was 7%. The energy deposited into the calorimeter (Fig. 5) is dominated by projectile spectator nucleons. The number of projectile participants (N_{pp}) is estimated by inverting the measured zero-degree energy (E_{ZCAL})

$$N_{pp}=197\times\left(1-\frac{E_{\mathrm{ZCAL}}}{E^{\mathrm{kin}}_{\mathrm{beam}}}\right). \tag{1}$$

For peripheral collisions, the calorimeter has a slight nonlinear response, with a 4% reduction in output for beam events that did not react compared to events that fragment

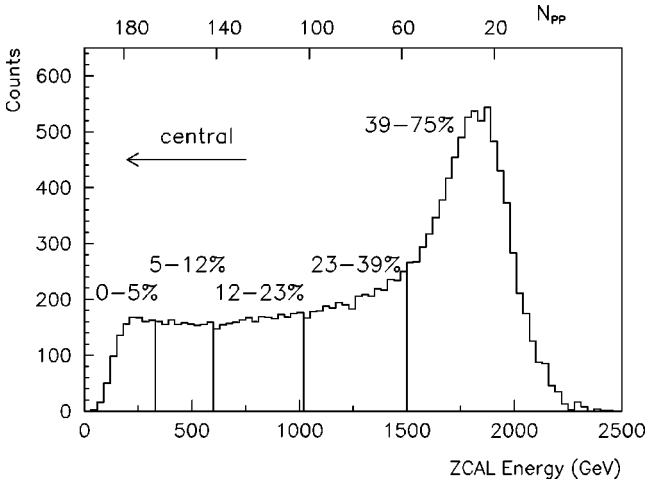

FIG. 5. The measured E_{ZCAL} distribution from interaction triggers in Au+Au reactions at 11.6A GeV/c. Target-out events have been subtracted. The event classes listed in Table I are separated by lines. The number of projectile nucleons N_{pp} obtained from E_{ZCAL} is indicated at the top of the figure. See text for details.

TABLE I. The five event classes used in this paper, listing the range of E_{ZCAL} values, the cross section for the event class, the percentage of the inelastic cross section ($\sigma_{\mathrm{int}}=6.8$ b), and the mean-value of the estimated number of projectile participants for that event class.

Event class	E_{ZCAL} range (GeV)	σ_{class}(mb)	% of σ_{int}	$\langle N_{pp}\rangle$
1	0–315	0–350	0–5	177
2	315–570	350–800	5–12	156
3	570–990	800–1566	12–23	124
4	990–1470	1566–2621	23–39	82
5	>1470	2621–5130	39–75	31

just upstream of the calorimeter. This leads to an uncertainty of up to eight in the value of N_{pp}, or 25%, only for the most peripheral event class.

Mesons entering the acceptance of the calorimeter also contribute to the measured E_{ZCAL} [19]. By passing events from a cascade model [4] through a simulation of the calorimeter, the meson energy contribution is estimated to be the equivalent of three projectile nucleons for the most central event class. It is proportionally smaller for less central bins. The mesonic contribution was not subtracted from E_{ZCAL}. N_{pp} should therefore be considered an experimental observable [defined by the measured E_{ZCAL}, Eq. (1)] and provides an estimate of the geometrical number of projectile participants.

By triggering the experiment on tracks in the spectrometer, the data can be sorted off-line into different centrality classes. Normalization is provided by prescaled interaction and beam triggers. For each class, the cuts on E_{ZCAL}, the corresponding mean value of N_{pp}, the measured cross section (after target-out correction) and the percentage of the total inelastic cross section ($\sigma_{\mathrm{int}}=6.8$ b), are listed in Table I. The most central event class is the same as was used in the measured E866 pion and proton spectra [9].

The two spectrometers have different tracking efficiencies and acceptances. The single-track reconstruction efficiency as a function of momentum for each spectrometer was determined by a Monte Carlo simulation. Events with one particle (pion, kaon, or proton) were first processed through a GEANT [20] model of each E866 spectrometer with hadronic interactions, decays, and multiple scattering processes included. The sampled momentum and angular distributions were flat. After the Monte Carlo simulation, the events were processed through the same reconstruction and particle identification code as real data. This provides the efficiency of the tracking algorithm for fully efficient hardware as a function of the momentum of the particle, and its values were 90–95 % for each spectrometer.

The Forward spectrometer reconstruction program requires that a track has at least three hit rows for each of two TPCs (six rows each). The detector efficiency $\epsilon_{\mathrm{TPC}}(x,y)$ is the probability that the TPCs satisfy this requirement. The efficiency maps of each row of the TPCs were determined from the fraction of missing hits in reconstructed tracks in the real data. Those efficiency maps were then used to calculate $\epsilon_{\mathrm{TPC}}(x,y)$ as function of track position. The value of ϵ_{TPC} was 93–100 %. The efficiencies of the drift chambers for both the Forward spectrometer and Henry Higgins were evaluated in a similar way, and were found to be very close to 100%.

Tracks are also lost because of hit blocking caused by the finite occupancy of chambers and TOF walls. For the Henry Higgins spectrometer this loss of tracks was estimated by embedding hits from isolated, single tracks from peripheral collisions into other events. The combined event was reanalyzed to see if the embedded track was still reconstructed by the tracking program. The resulting blocking-induced inefficiency was parameterized as a function of the overall occupancy of the Henry Higgins spectrometer and as a function of position both in front and behind the magnet. For the most central event class and tracks at forward angles, the blocking inefficiency was $40\pm10\%$. This inefficiency reduces to $10\pm5\%$ at back angles.

In the Forward spectrometer the loss of tracks due to hit-blocking was dominated by earlier hits in the TOF wall. This probability was determined from the data for each centrality class and angle setting as a function of the position and timing in the TOF wall. The efficiency ranged from 70–100 %. In addition, the hit-blocking effects in the tracking stations were studied by embedding Monte Carlo tracks in the real data. The inefficiency was determined as a function of track multiplicity and was less than 10% in the most central event class. The PID efficiency is the probability that a track fall in the PID window for each spectrometer, and is determined from the shape of the PID window (Figs. 3 and 4).

The survival fraction is the probability that a particle reaches the TOF wall before it decays. The expected value is $\exp(-Lm/c\tau p)$ for an ideal detector, but can be closer to unity since some particles that decay in flight can still be accepted by the reconstruction program. The survival fraction was studied for each spectrometer by a Monte Carlo simulation and was found to be very close to the expected value $\exp(-Lm/c\tau p)$ for kaons. The data were corrected on a track-by-track basis for each inefficiency; single-track reconstruction, chamber inefficiency, loss of tracks due to hit blocking, PID inefficiency and particle decay.

The systematic uncertainty on the normalization of the measured invariant spectra and rapidity distributions is dominated by uncertainty of the single-track efficiency and loss of tracks due to hit blocking. The tracking uncertainty increases from 5–10 % the closer to midrapidity and the more central the event class. For peripheral collisions, there is a 10% uncertainty in the cross-section of the event class. This reduces to 5% for central collisions. There are small contributions to the uncertainty from the acceptance of the spectrometer and particle identification losses. This leads to a total systematic uncertainty in the normalization of 15% independent of centrality.

The systematic uncertainty on the inverse slope parameters is estimated to be 5% and is dominated by uncertainty in the tracking efficiency and acceptance. A cross check on the data is that the spectra from each spectrometer, with different tracking algorithms and efficiencies, agree very well (see Sec. III).

III. SPECTRA AND YIELDS

In Figs. 6–15 the invariant cross-sections, divided by the reaction cross-section for the event class, are plotted for ka-

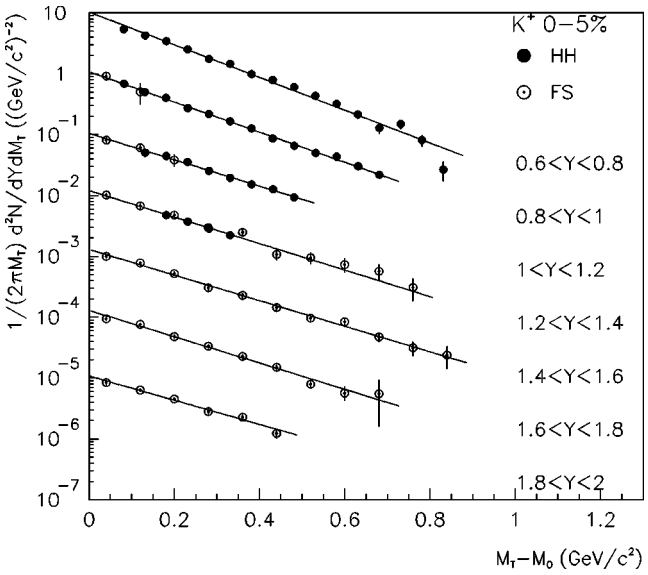

FIG. 6. The invariant yield of K^+ as a function of transverse mass for different slices in rapidity for the most central 5% of Au+Au reactions at 11.6A GeV/c. The data from the Henry Higgins spectrometer are shown as filled circles, while the kaons from the Forward spectrometer are shown as open circles with a dot. The most backward rapidity is the correct scale, successive spectra have been divided by 10 for clarity. The errors are statistical only. The systematic errors are described in Sec. II.

ons as a function of transverse mass and rapidity. Transverse mass is $m_t=\sqrt{p_t^2+m_0^2}$, where p_t is the transverse momentum and m_0 is the rest mass of the particle. These spectra are the differential yield of kaons per event.

For clarity, the spectra are divided by a factor of ten for each rapidity slice. Kaons in the Henry Higgins spectrometer are indicated by filled circles, while kaons in the Forward spectrometer are denoted by open circles with a dot. The acceptances of the spectrometers complement each other.

To test whether the data from the two spectrometers are consistent with each other the following two procedures were used. First the spectra from the Forward spectrometer

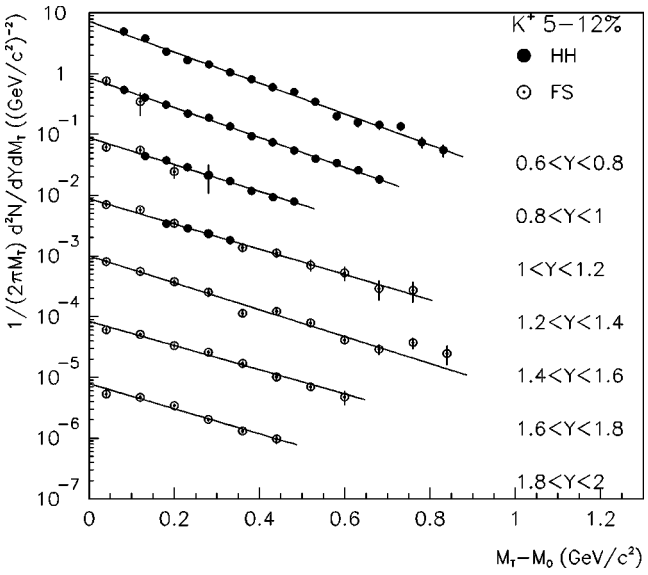

FIG. 7. Same as Fig. 6, but for the 5–12 % central reactions.

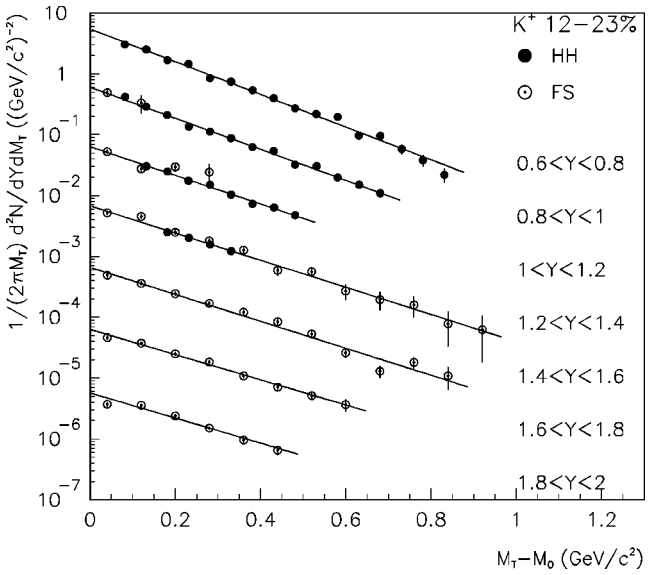

FIG. 8. Same as Fig. 6, but for the 12–23 % central reactions.

were fitted with an exponential in m_t. A χ^2 statistic with respect to this fit was calculated for the Henry Higgins data that are within the acceptance of the Forward spectrometer. Over all the event classes and the two rapidity slices ($1.0<y<1.2$ and $1.2<y<1.4$) the average χ^2/point was 1.2. Reversing the roles of the spectrometers, i.e., fitting the Henry Higgins spectra and calculating the χ^2 of the Forward spectrometer data points, produced an average χ^2/point of 1.7. The low values of χ^2/point indicate that the spectra are consistent with each other.

In the second test of the consistency of the spectra, the relative normalization between the Henry Higgins data and the Forward spectrometer data was allowed to vary. This was an additional parameter in the exponential fit of each spectrum that has data from both spectrometers. The fits with a free relative normalization reduced the χ^2 by an average of 1.5. For the relative normalization to be statistically significant this decrease would need to be considerably larger than

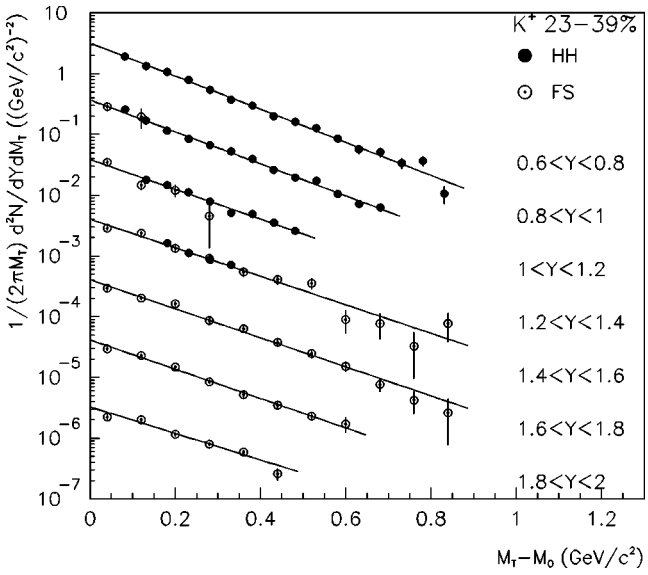

FIG. 9. Same as Fig. 6, but for the 23–39 % central reactions.

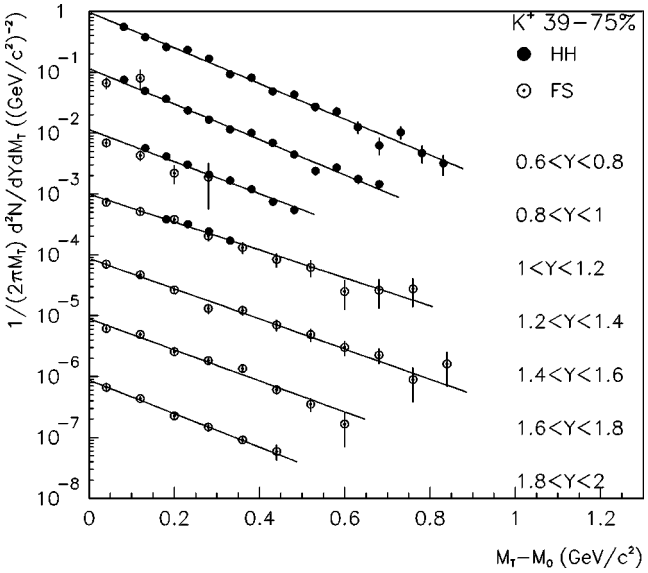

FIG. 10. Same as Fig. 6, but for the 39–75% central reactions.

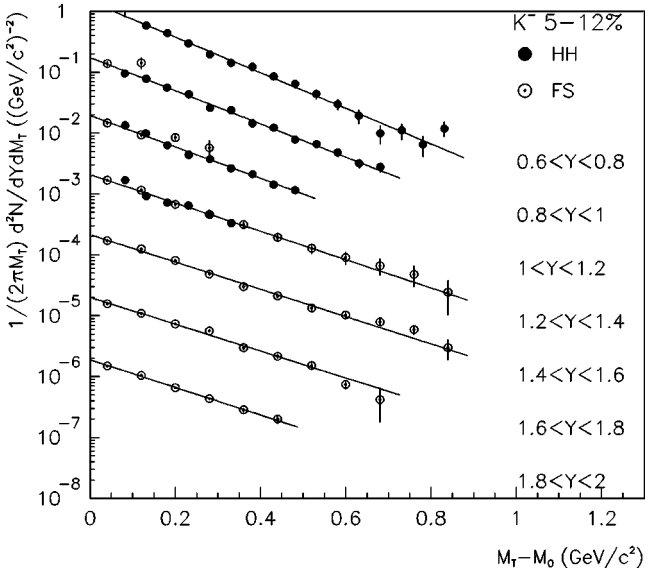

FIG. 12. Same as Fig. 11, but for the 5–12 % central reactions.

one. The mean of the relative normalization from the thirty spectra is 1.00 with a rms of 0.14. The observation that the mean normalization is near unity and that the decrease in χ^2 is small, confirms that the data from the two spectrometers are consistent with each other.

The spectra in Figs. 6–15 were fit with the following exponential in m_t using both the Forward spectrometer and the Henry Higgins data:

$$\frac{1}{2\pi m_t}\frac{d^2N}{dm_t dy}=\frac{dN/dy}{2\pi(Tm_0+T^2)}e^{-(m_t-m_0)/T}. \qquad (2)$$

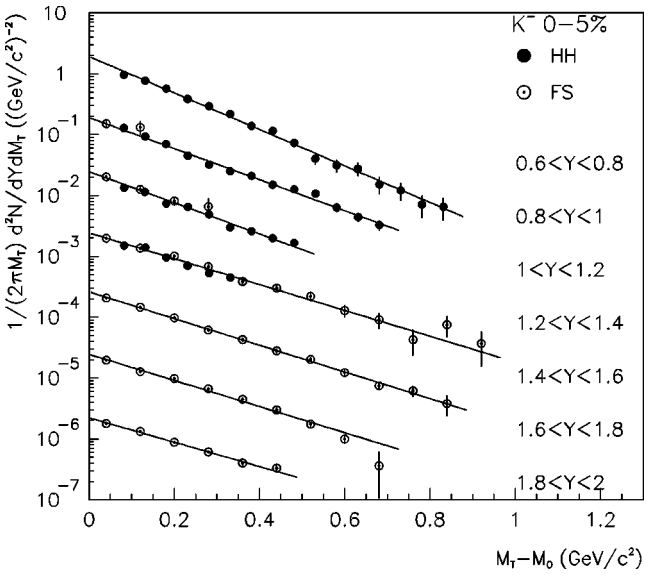

FIG. 11. The invariant yield of K^- as a function of transverse mass for different slices in rapidity for the most central 5% of Au+Au reactions at 11.6A GeV/c. The data from the Henry Higgins spectrometer are shown as filled circles, while the kaons from the Forward spectrometer are shown as open circles with a dot. The most backward rapidity is the correct scale, successive spectra have been divided by 10 for clarity. The errors are statistical only. The systematic errors are described in Sec. II.

In the fits the data points are weighted by their statistical errors only. The relative normalization of the spectra from the two spectrometers was fixed at unity. The exponential fits reproduce the spectra well and provide the inverse slope parameter T and the rapidity density dN/dy in that rapidity slice. These fits combine information from both spectrometers. The values for these parameters for both K^+ and K^- are tabulated in Tables II and III as a function of rapidity and centrality.

As one check on the systematics on obtaining the rapidity density, a Boltzmann form was also fitted to the m_t spectra:

$$\frac{1}{2\pi m_t}\frac{d^2N}{dm_t dy}=\frac{dN/dy}{2\pi(T_B m_0^2+2m_0T_B^2+2T_B^3)}m_t e^{-(m_t-m_0)/T_B}, \qquad (3)$$

where T_B and dN/dy were free parameters. The extracted dN/dy values were systematically 3% lower than the dN/dy

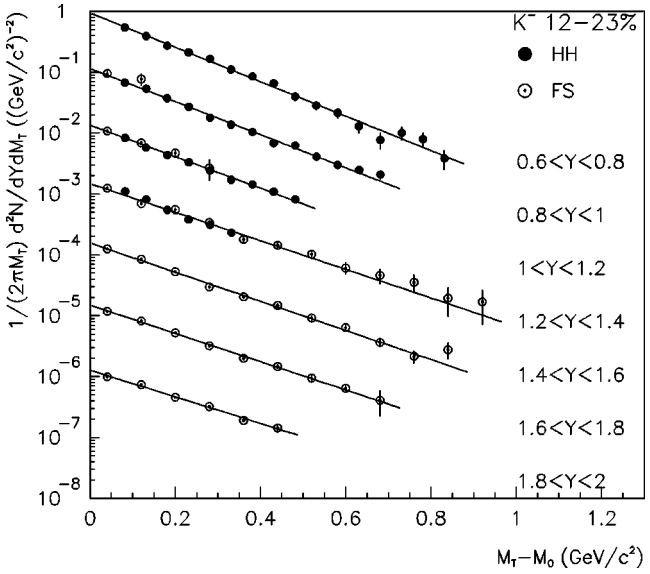

FIG. 13. Same as Fig. 11, but for the 12–23 % central reactions.

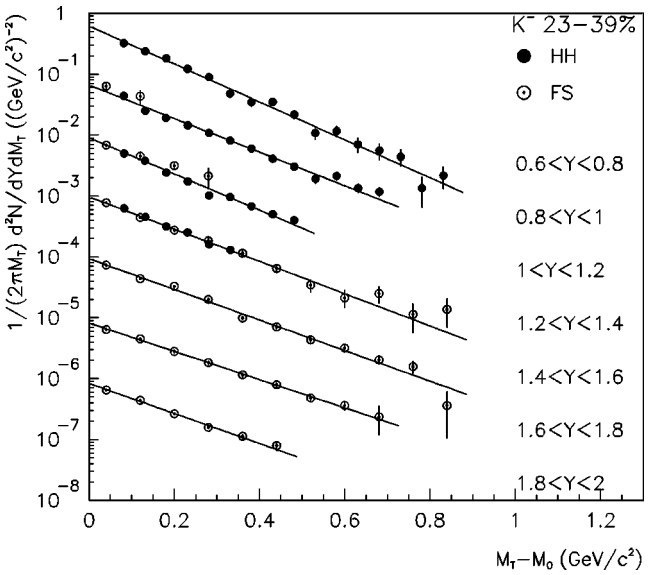

FIG. 14. Same as Fig. 11, but for the 23–39 % central reactions.

from exponential fits. The χ^2 for the Boltzmann and exponential fits were similar. Exponential fits will be used throughout this paper.

The errors on the parameters T and dN/dy from the exponential fits were obtained with the standard method from the variation of χ^2 around the minimum. For fits with $\chi^2/N_{\mathrm{DF}}>1$, these errors are likely to be underestimated. Following the recommendation of the Particle Data Group [21], the errors on the fitted parameters (dN/dy and T) are increased by a scale factor of $(\chi^2/N_{\mathrm{DF}})^{1/2}$ with a minimum scale factor of unity.

Figure 16 shows the dN/dy distributions for K^+ and K^-. The different centrality groups are indicated by different symbols, with kaons from the most central collisions having the largest dN/dy. The open symbols in Fig. 16 are the data points reflected about midrapidity. The dN/dy distributions are approximately Gaussian in shape. The distributions for K^- are narrower than those for K^+ (discussed in more detail in Sec. IV).

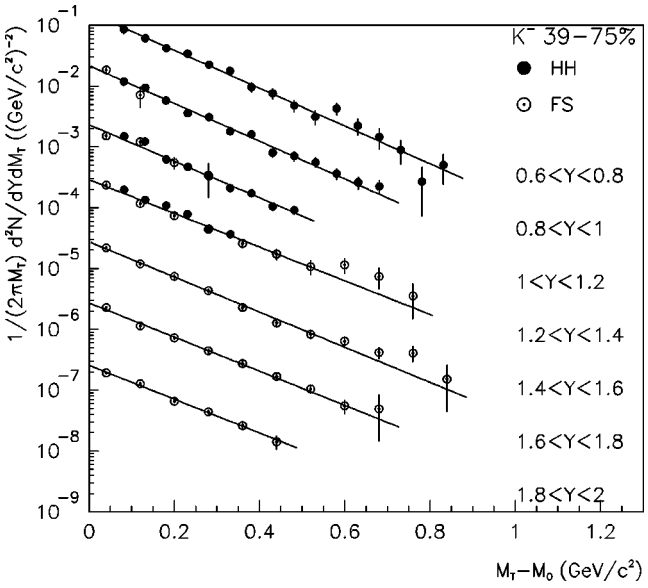

FIG. 15. Same as Fig. 11, but for the 39–75 % central reactions.

TABLE II. The dN/dy and inverse slope distributions for K^+ for each centrality class defined in Table I. The errors are statistical only.

y	$K^+ dN/dy$	$K^+ T$ (GeV)	χ^2/N_{DF}
	Event class 1		
0.7	6.89±0.29	0.161±0.004	23.8/14
0.9	7.94±0.24	0.175±0.004	3.4/13
1.1	9.16±0.23	0.201±0.008	3.6/ 9
1.3	10.47±0.28	0.199±0.009	6.9/12
1.5	11.79±0.37	0.207±0.007	5.5/ 9
1.7	11.34±0.33	0.201±0.008	7.7/ 7
1.9	10.56±0.39	0.219±0.014	4.2/ 4
	Event class 2		
0.7	5.19±0.18	0.171±0.004	15.1/14
0.9	6.39±0.18	0.176±0.004	4.1/13
1.1	7.53±0.18	0.196±0.007	9.5/10
1.3	8.07±0.22	0.209±0.010	4.8/12
1.5	8.49±0.40	0.196±0.010	18.6/ 9
1.7	8.17±0.29	0.218±0.010	8.1/ 6
1.9	7.34±0.40	0.210±0.019	9.1/ 4
	Event class 3		
0.7	3.63±0.12	0.162±0.004	16.7/14
0.9	4.28±0.12	0.170±0.004	10.5/13
1.1	4.98±0.13	0.184±0.007	12.0/10
1.3	5.68±0.14	0.195±0.007	13.6/14
1.5	5.60±0.24	0.196±0.008	17.0/ 9
1.7	5.85±0.18	0.210±0.009	7.6/ 6
1.9	5.31±0.31	0.211±0.020	13.3/ 4
	Event class 4		
0.7	2.09±0.07	0.159±0.004	11.4/14
0.9	2.53±0.08	0.165±0.004	8.5/13
1.1	2.88±0.09	0.177±0.008	14.6/10
1.3	3.17±0.09	0.185±0.008	16.1/13
1.5	3.12±0.12	0.182±0.006	10.8/ 9
1.7	3.16±0.10	0.180±0.007	6.9/ 6
1.9	2.83±0.17	0.199±0.020	11.9/ 4
	Event class 5		
0.7	0.58±0.02	0.148±0.004	13.9/14
0.9	0.69±0.03	0.149±0.005	15.5/13
1.1	0.78±0.03	0.165±0.008	17.0/10
1.3	0.81±0.03	0.190±0.010	7.2/12
1.5	0.64±0.03	0.175±0.009	6.2/ 9
1.7	0.63±0.03	0.170±0.010	9.3/ 6
1.9	0.57±0.03	0.158±0.011	1.3/ 4

Systematically the forward-rapidity dN/dy data points are 5–10 % lower than their symmetric partners at back rapidity implying this level of consistency in the measurements. For the most peripheral event class, the forward rapidity dN/dy K^+ data points are 20% lower than their symmetric back-rapidity partners. Small gain drifts in the calorimeter may have changed the selection of peripheral events. The symmetry of dN/dy distributions is unaffected by the choice of the fitting function [Eqs. (2) or (3)] used to fit the m_T spectra.

TABLE III. The dN/dy and inverse slope distributions for K^- for each centrality class defined in Table I. The errors are statistical only.

y	$K^- dN/dy$	$K^- T$ (GeV)	χ^2/N_{DF}
	Event class 1		
0.7	1.12±0.05	0.145±0.004	5.8/14
0.9	1.36±0.05	0.170±0.005	10.1/13
1.1	1.74±0.05	0.170±0.006	9.1/11
1.3	2.18±0.06	0.204±0.007	12.6/16
1.5	2.24±0.05	0.198±0.004	3.1/ 9
1.7	2.17±0.07	0.202±0.008	14.8/ 7
1.9	2.15±0.06	0.217±0.009	2.9/ 4
	Event class 2		
0.7	0.87±0.04	0.149±0.005	10.0/14
0.9	1.14±0.04	0.159±0.004	11.1/13
1.1	1.36±0.04	0.169±0.006	11.7/11
1.3	1.65±0.04	0.186±0.006	8.4/16
1.5	1.79±0.05	0.194±0.005	13.5/ 9
1.7	1.71±0.05	0.197±0.007	12.3/ 7
1.9	1.56±0.04	0.191±0.007	1.3/ 4
	Event class 3		
0.7	0.59±0.02	0.154±0.004	7.5/14
0.9	0.75±0.02	0.160±0.004	9.7/13
1.1	0.94±0.02	0.168±0.005	4.5/11
1.3	1.16±0.03	0.185±0.006	19.1/16
1.5	1.20±0.03	0.182±0.004	11.5/ 9
1.7	1.19±0.02	0.187±0.004	3.8/ 7
1.9	1.10±0.03	0.199±0.009	6.7/ 4
	Event class 4		
0.7	0.34±0.02	0.139±0.004	12.5/14
0.9	0.43±0.02	0.158±0.006	16.9/13
1.1	0.53±0.02	0.146±0.006	18.8/11
1.3	0.65±0.02	0.164±0.005	7.5/15
1.5	0.67±0.02	0.173±0.005	16.7/ 9
1.7	0.65±0.01	0.187±0.005	2.5/ 7
1.9	0.62±0.02	0.176±0.007	4.4/ 4
	Event class 5		
0.7	0.09±0.01	0.140±0.005	9.7/14
0.9	0.12±0.01	0.140±0.005	10.4/13
1.1	0.13±0.01	0.145±0.006	15.0/11
1.3	0.19±0.01	0.157±0.007	18.7/14
1.5	0.17±0.01	0.150±0.005	10.9/ 9
1.7	0.17±0.01	0.155±0.005	7.7/ 7
1.9	0.16±0.01	0.156±0.006	4.4/ 4

The inverse slope parameters (from the exponential fits to the m_t spectra) for both K^+ and K^- are largest near midrapidity. This is shown in Fig. 17 for K^+ and K^- from central collisions and tabulated for all centralities in Tables II and III.

The inverse slopes increase with centrality, especially near midrapidity where T_{K^+} increases from 170 to 210 MeV. In Fig. 18 three representative rapidity slices from Tables II and III are plotted versus the number of projectile participants N_{pp}. The K^+ inverse slopes tend to be larger than those of the K^- by about 10 to 20 MeV (discussed in more detail in Sec. IV).

These inverse slopes from central Au+Au reactions are similar to the values measured in central Si+A collisions for kaons at midrapidity ($T\sim 200$ MeV) [8]. The inverse slopes from Au+Au peripheral reactions can be compared to $p+p$ reactions at 12 GeV/c, where the data of Rossi *et al.* [22,23] correspond to inverse slope parameters of an exponential m_t spectrum of $T=143$, $T=132$ MeV for K^+ and K^-, respectively. These inverse slopes are slightly smaller than the inverse slopes from peripheral Au+Au reactions ($T_{K^+}\sim 160$ MeV and $T_{K^-}\sim 150$ MeV). In $p+p$ reactions the spectra for K^+ are slightly harder than the spectra for K^-.

The dN/dy distributions from Au+Au (Fig. 16) were fit with Gaussians. Each fit was constrained to be centered at midrapidity ($y=1.6$) and all data points in the dN/dy distribution were included in the fit. The extracted widths of the K^- distributions σ_{K^-} range from 0.72 to 0.76 units of rapidity. These widths are smaller than the widths from the K^+ distributions σ_{K^+} which range from 0.86 to 0.99 units of rapidity.

The second parameter in the fit was the total yield of kaons per event. The extrapolation out to back rapidities introduces an additional 5% systematic error to the total yields. Excluding the most forward rapidity point from the fit changed the total yield by less than 2%. To complement the total yield, the fiducial yield of kaons is also calculated, defined to be

$$\text{fiducial yield} = \sum \frac{dN}{dy} dy, \quad 0.6 < y < 2.0 \tag{4}$$

which is the sum of the dN/dy distribution in the region where the spectrometers have acceptance. The total yield, the sigma of the Gaussian and the fiducial yields are tabulated in Table IV for each event class.

For the most peripheral event class, the 20% asymmetry in the dN/dy distribution makes it difficult to extract a total yield. The total yield of both K^+ and K^- in the peripheral event class has been estimated in two ways: (1) using only the back rapidity dN/dy data in the Gaussian fit and (2) keeping the width of the Gaussian fixed at the value from the event class number four (Table IV). The yields from these two techniques were similar and were averaged. The difference between the techniques was used to estimate the uncertainty of the peripheral kaon yields listed in Table IV.

The K^+ and K^- total yields are shown versus the number of projectile participants N_{pp} in Fig. 19. The yield for both kaon species increases nonlinearly with N_{pp}. The total yield for K^+ and K^- in central Au+Au collisions is 24.2 ± 0.9 and 4.14 ± 0.09, respectively. The yield per projectile participant is highest in the most central collisions. This is emphasized in Fig. 20 where the kaon yield per projectile participant is plotted versus the number of projectile participants.

The hatched boxes in Fig. 20 are the kaon yields expected from $N+N$ collisions at the same beam energy, where yield is defined to be the production cross section divided by the inelastic cross section. The yields from $N+N$ collisions are the isospin-weighted average of yields from $p+p$, $n+p$,

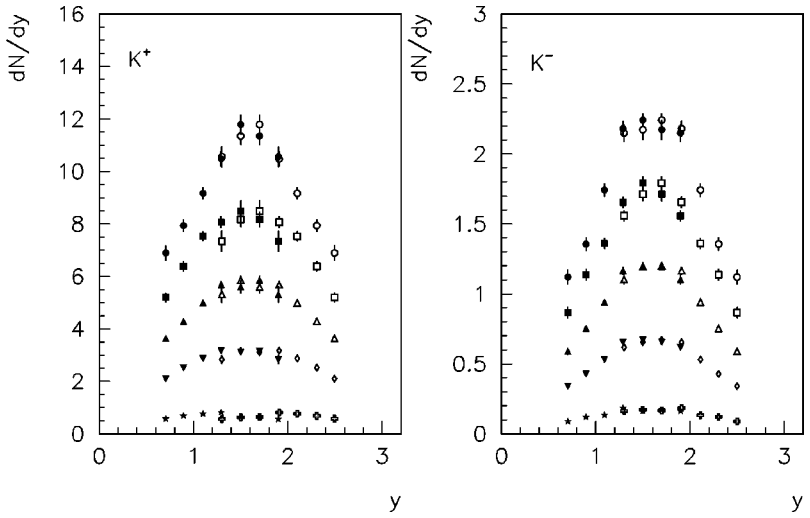

FIG. 16. The dN/dy distributions of kaons for different centrality classes (listed in Table I) of Au+Au reactions at 11.6A GeV/c. The distributions are from fits to invariant cross sections including data from both E866 spectrometers. The K^+ spectra are in the left panel and the K^- spectra are in the right panel. The circles are from the 0–5 % centrality class, the squares from the 5–12 % centrality class, the triangles from the 12–23 % centrality class, the inverted triangles from the 23–39 % centrality class, and the stars from the 39–75 % centrality class. The open symbols are the data points reflected around midrapidity. The errors are statistical only. The systematic errors are described in Sec. II.

and $n+n$ collisions. For details on the calculation of these yields and cross sections see the Appendix.

The measured K^+ yield of 0.137 per projectile participant in central Au+Au is 3.7 ± 0.5 times the yield in the $N+N$ collisions, i.e., kaon production is enhanced. The enhancement for K^- production is slightly less, with the central Au +Au yield of 0.023 per projectile participant being 2.5 ±0.4 times the yield from $N+N$ collisions. These enhancements suggest that the majority of kaons in central reactions come from secondary collisions.

Both K^+ and K^- yields increase with centrality in a similar manner. The increase in kaon yields with centrality is very steady. There is no indication of an onset, or sudden change in kaon production. It is difficult to quantify this. To set an upper limit on a change in kaon production requires some assumptions on the expected normal increase of kaon production and on the centrality class where the change may occur. The yield of kaons versus N_{pp} from the four more peripheral event classes has been fitted with two functional forms, a power law (two free parameters), or a quadratic in N_{pp} (three free parameters). These fits included the point-to-point 5% systematic uncertainty of the yields. The fit is extrapolated to the most central event class (Fig. 21), where the measured central kaon yield is consistent with the extrapolation. Taking into account the variation from the different functional forms and the uncertainty of the extrapolation, an upper limit is set for additional kaon production in the most central events. At the 90% C.L. any additional kaon production is less than $7K^+$ per event and $0.9K^-$ per event.

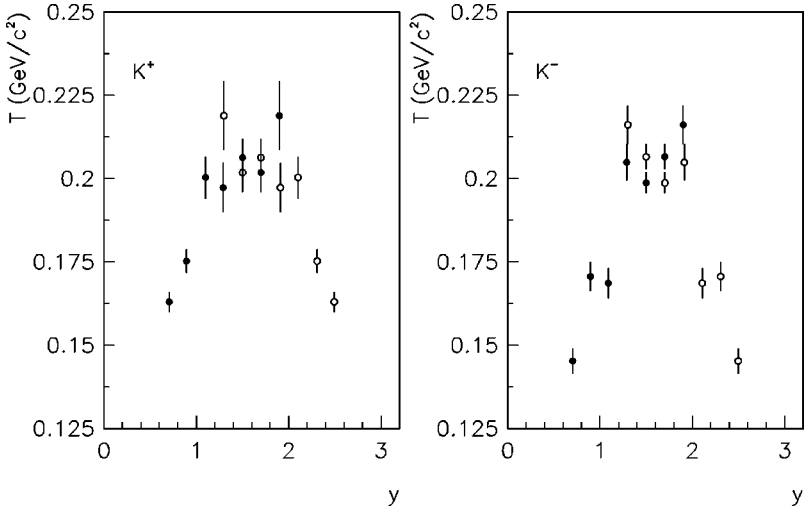

FIG. 17. The inverse slope parameters of kaons versus rapidity for the most central 5% of Au+Au reactions at 11.6A GeV/c. The slope parameters are from fits to invariant cross sections including data from both E866 spectrometers. The K^+ inverse slopes are in the left panel and the K^- inverse slopes are in the right panel. The open symbols are the data points reflected around midrapidity. The errors are statistical only. The systematic errors are described in Sec. II.

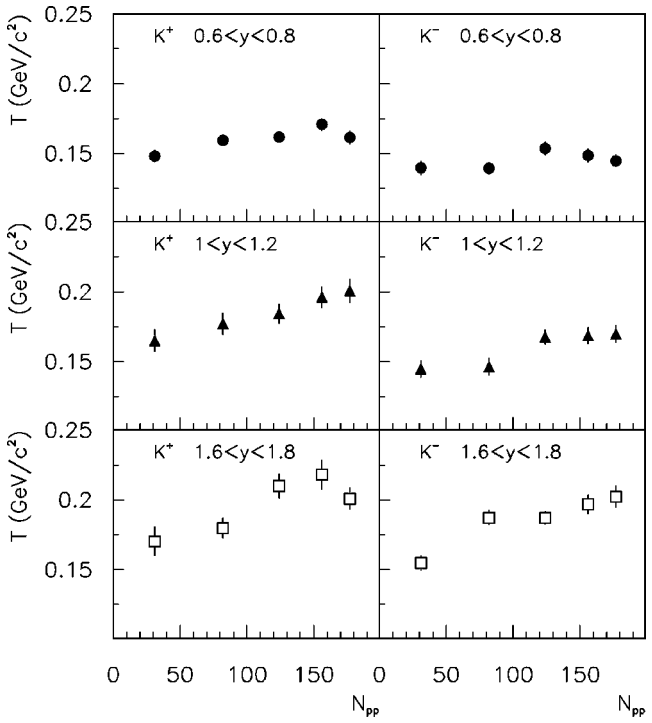

FIG. 18. The inverse slope parameters of kaons versus the experimental estimate of the number of projectile participants N_{pp} for different slices of rapidity in Au+Au reactions at 11.6A GeV/c. The slope parameters are from fits to invariant cross sections including data from both E866 spectrometers. The K^+ inverse slopes are in the left panel and the K^- inverse slopes are in the right panel. The errors are statistical only. The systematic errors are described in Sec. II.

IV. COMPARISON OF K^- AND K^+ EMISSION

The physics of K^+ and K^- production are very different. They have different energy thresholds of production ($K^+\sqrt{s}=2.55$ GeV and $K^-\sqrt{s}=2.86$ GeV). K^- are strongly absorbed in nuclear matter, with the s-quark exchange reaction $K^-+N\rightleftharpoons\Lambda+\pi$ having a cross section of approximately 20 mb for $p_K<1$ GeV/c. The inelastic cross section in K^++N scattering is less than 4 mb for $p_K<1$ GeV/c. There is evidence from kaonic atoms [14] that the K^- nuclear potential is attractive. Insight into these three differences (production, absorption, in-medium properties) can be gained by comparing K^- and K^+ yields and spectra.

The ratio of the K^- and K^+ total yields as a function of N_{pp} is plotted in Fig. 22. This ratio is independent of the measured range of centrality. Whatever mechanism drives the enhancement of kaons, it similarly affects both K^+ and K^-. Note that the most peripheral event class contains events occurring in the range 39–75 % of the inelastic cross

TABLE IV. The total yield, Gaussian σ, the $\chi^2/N_{\rm DF}$ from the Gaussian fits of the dN/dy distributions, and fiducial yields for K^+ and K^- for each centrality class defined in Table I. For the peripheral bin the error includes the systematic uncertainty estimated from the difference in kaon yield using two techniques (see text). For the other centralities the errors are statistical only.

Event class	Total yield K^+	σK^+	$\chi^2/N_{\rm DF}$	Fiducial yield K^+
1	24.2±0.9	0.86±0.03	6.6/5	13.6±0.2
2	19.7±0.6	0.93±0.04	5.6/5	10.2±0.2
3	13.3±0.4	0.91±0.03	3.1/5	7.1±0.1
4	8.0±0.3	0.99±0.04	4.6/5	3.95±0.06
5	2.0±0.3			0.94±0.02

Event Class	Total yield K^-	σK^-	$\chi^2/N_{\rm DF}$	Fiducial yield K^-
1	4.14±0.09	0.72±0.02	9.7/5	2.59±0.03
2	3.29±0.08	0.75±0.02	6.0/5	2.02±0.02
3	2.23±0.04	0.73±0.02	5.0/5	1.39±0.01
4	1.28±0.03	0.76±0.02	6.7/5	0.78±0.01
5	0.34±0.02			0.206±0.003

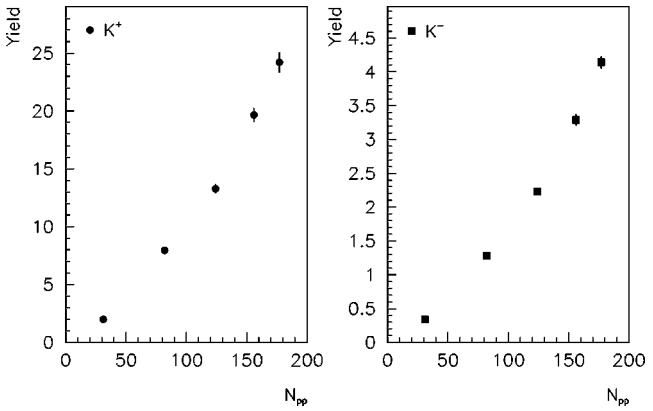

FIG. 19. The total yields of kaons versus the experimental estimate of the number of projectile participants N_{pp} in Au+Au reactions at 11.6A GeV/c. Each total yield is from a Gaussian fit to the kaon dN/dy distribution. The K^+ yields are in the left panel and the K^- yields are in the right panel. For the peripheral bin the error bar includes the systematic uncertainty estimated from the difference in kaon yield using two techniques (see text). For the other centralities the errors are statistical only.

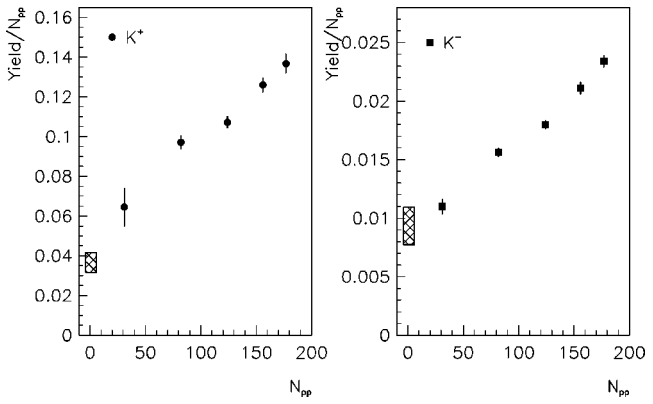

FIG. 20. The total yields of kaons per projectile participant versus the number of projectile participants N_{pp} in Au+Au reactions at 11.6A GeV/c. Each total yield is from a Gaussian fit to the kaon dN/dy distribution. The K^+ yields are in the left panel and the K^- yields are in the right panel. For the peripheral bin the error bar includes the systematic uncertainty estimated from the difference in kaon yield using two techniques (see text). For the other centralities the errors are statistical only. The box on the left is an estimate of the kaon yield from the initial $N+N$ collisions.

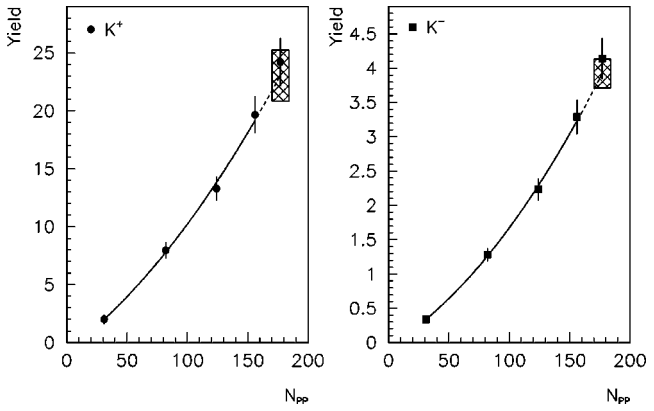

FIG. 21. The total yields of kaons versus the number of projectile participants N_{pp} in Au+Au reactions at 11.6A GeV/c. The error bars include the 5% point-to-point systematic uncertainty. The solid line is a quadratic fit to the yields in the first four centrality classes, and the dashed line indicates the extrapolation to the most central data point. The box indicates a $\pm\sigma$ uncertainty in the extrapolation.

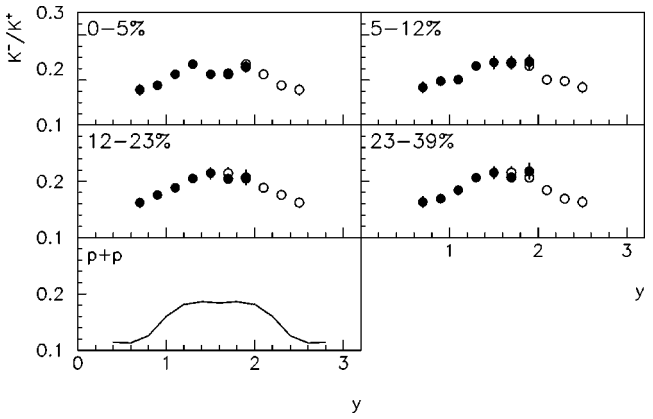

FIG. 23. The K^-/K^+ ratio of the rapidity distributions for the first four centrality classes (Table I) in Au+Au reactions at 11.6A GeV/c. The open symbols are the data points reflected around midrapidity. The errors are statistical only. The systematic errors are described in Sec. II. The bottom panel is the K^-/K^+ ratio from $p+p$ collisions adapted from Fesefeldt *et al.* [28].

section. The hatched box on the left indicates the K^-/K^+ ratio from the isospin-weighted N-N collisions at the same energy. The ratio from N-N collisions is higher than the ratio in the most peripheral Au+Au event class.

The top four panels of Fig. 23 show the ratio of dN/dy distributions for K^-/K^+ for different centrality classes in Au+Au collisions. This ratio reaches a maximum near midrapidity. Equivalently the K^-dN/dy distribution is narrower than the K^+ distribution (see also Table III).

The K^-/K^+ ratio has a very similar dependence on rapidity for all centralities. For reference, the bottom panel is the K^-/K^+ ratio from $p+p$ reactions at 12 GeV/c adapted from Fesefeldt *et al.* [28] (this has not been isospin averaged). The $p+p$ K^-/K^+ ratio also has a maximum at midrapidity, possibly due to the smaller phase space available to K^- which reduces K^- production away from midrapidity.

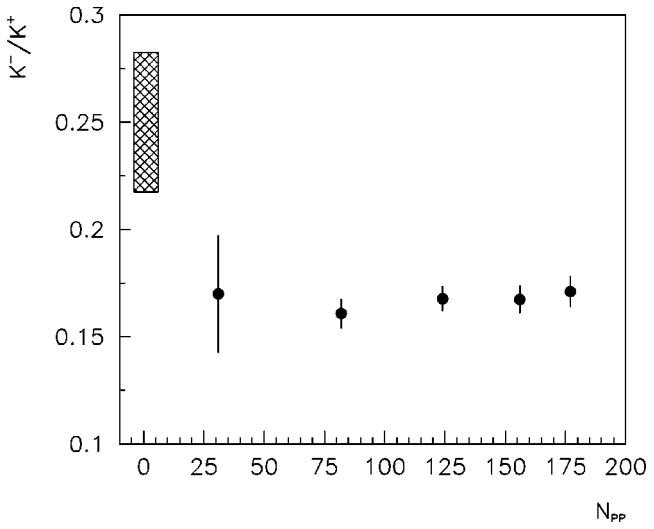

FIG. 22. The K^-/K^+ ratio of total yields versus the experimental estimate of the number of projectile participants N_{pp} in Au+Au reactions at 11.6A GeV/c. For the peripheral bin the error bar includes the systematic uncertainty estimated from the difference in kaon yield using two techniques (see text). For the other centralities the errors are statistical only. The box is an estimate of the ratio from initial $N+N$ collisions.

In Sec. III it was discussed that many of the kaons produced in Au+Au collisions come from secondary collisions. Given the similarity of the $p+p$ and Au+Au K^-/K^+ rapidity distributions, these secondary collisions seem to retain the wider rapidity width of K^+ production.

In Fig. 24 the difference in inverse slopes, $\Delta T = T_{K^+} - T_{K^-}$, is plotted versus rapidity for each centrality class. In noncentral reactions the K^- inverse slope parameter is slightly smaller than the K^+ inverse slope by 10–20 MeV, comparable to the difference in $p+p$ reactions. However, for central reactions near midrapidity, the K^- and $K^+ m_t$ distribution are very similar. At these rapidities, either the difference in energy threshold for K^- and K^+ production has little effect on the final m_t distribution, or scattering after kaon production removes any difference between K^- and K^+ spectra. This rescattering would be strongest where the pion and proton dN/dy is largest, i.e., at midrapidity and for central collisions.

Although for the most central collisions and in the most central slice of rapidity the kaon spectra do become similar, the overall difference between the K^+ and K^- rapidity densities and the transverse spectra rule out global-equilibrium thermal models [24–27]. These models assume the thermal parameters are uniform across the emitting system and that all particles are in kinetic equilibrium. For a system at kinetic equilibrium, there is sufficient scattering so that the spectra of equal mass particles are identical in shape, even if the system is expanding. A model that assumes global equilibrium is ruled out by the measured data. It may, however, be possible to reconcile these data with a modified thermal model.

Note that absorption of K^- does not seem to drive the difference in the K^+ and K^- spectral shapes. Low m_t K^- should be preferentially absorbed, thereby causing a larger inverse slope for K^- compared to K^+. This is not observed.

Several predictions suggest that in-medium effects could tilt the spectra, reducing the K^- inverse slope and increasing the K^+ inverse slope [15]. Because the amount of matter at

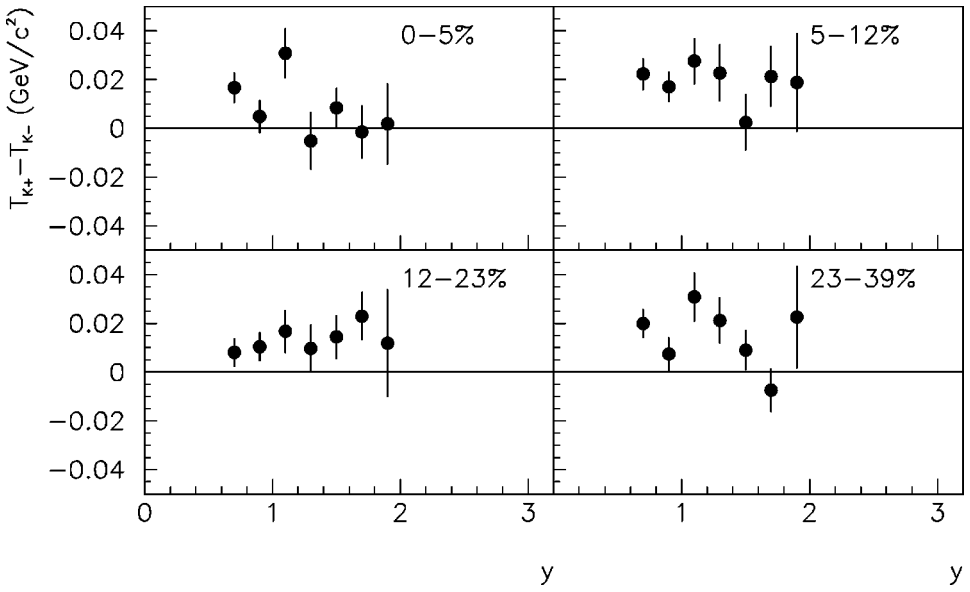

FIG. 24. The difference in inverse slope parameter $T_{K^+}-T_{K^-}$ versus y for the first four centrality classes (Table I) in Au+Au reactions at 11.6A GeV/c. The errors are statistical only. The systematic errors are described in Sec. II.

high density increases with centrality, this could drive the difference in inverse slopes to be largest for the most central reactions and at midrapidity. Although the K^+ temperature is significantly higher than K^- in midcentral reactions (as found in $p+p$), the difference disappears at high centrality and at midrapidity, opposite to the trends expected from medium effects.

V. KAON TO PION RATIOS

In a previous publication [9], the E866 Collaboration has reported on the pion yields from central Au+Au collisions at 11.6A GeV/c. The centrality selection was the same as the most central event class of this paper. To compare to the kaon results, a pion fiducial yield over the same rapidity range ($0.6<y<2.0$) was extracted from the data in reference [9]. The π^+ fiducial yield is 69.2 ± 0.6 and the π^- fiducial yield is 85.1 ± 0.6, where the uncertainties are statistical only.

Combined with the kaon yields in Table IV, the kaon to pion ratios are $K^+/\pi^+=0.197\pm0.003\pm0.010$ and $K^-/\pi^-=0.0304\pm0.0004\pm0.0015$, where the quoted errors are the statistical and systematic uncertainties, respectively. The systematic uncertainty in the K/π ratio is dominated by uncertainties in the normalization between the different angle settings needed to cover the same rapidity range for kaons and pions.

In central Si+A reactions at 14.6A GeV/c [8] the measured K^+/π^+ ratio between $0.5<y<2.3$ for Al, Cu, and Au targets is 0.130 ± 0.008, 0.163 ± 0.006, and 0.185 ± 0.007, respectively. The data from the Si and Au beams show a steady increase in K^+/π^+ with increasing size of the system. This continues the trend measured by our collaboration in $p+A$ reactions at 14.6A GeV/c [7] where the K^+/π^+ ratio between $1.2<y<1.4$ increases with the target mass number (for Be, Al, Cu, and Au targets $K^+/\pi^+=0.078\pm0.004$, 0.099 ± 0.005, 0.106 ± 0.006, and 0.125 ± 0.006, respectively). These results are summarized in Fig. 25, where the K^+/π^+ ratio is plotted for each beam and target combination. The ratio steadily increases with system size. Note that the Au beam energy (11.6A GeV/c) is lower than the Si beam energy (14.6A GeV/c). Over this energy range the K^+/π^+ ratio decreases by 14% in $p+p$ reactions. Such a correction is not applied to the Au+Au data because the dependence on beam energy is likely to be different for heavy-ion reactions compared to proton reactions. It is also noted that the isospin changes with collision system.

The K^-/π^- ratio from central Si+A reactions at 14.6A GeV/c [8] between $0.8<y<2.0$ for Al, Cu, and Au targets is 0.042 ± 0.013, 0.050 ± 0.013, and 0.038 ± 0.010, respectively. The K^-/π^- ratio from $p+A$ reactions at 14.6A GeV/c [7] between $1.0<y<2.0$ for Be, Al, Cu, and Au targets is 0.023 ± 0.007, 0.029 ± 0.010, 0.025 ± 0.007, and

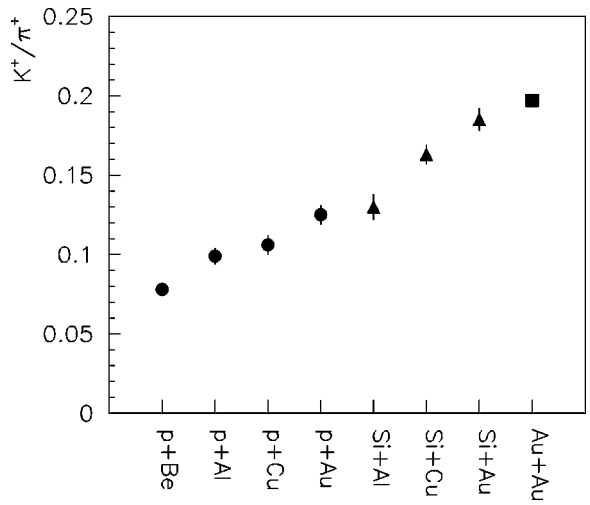

FIG. 25. The K^+/π^+ ratio for different beam target combinations. The Au+Au (11.6A GeV/c) datum is from this paper. The $p+A$(14.6A GeV/c) and Si+A(14.6A GeV/c) points are from Refs. [7] and [8], respectively. Each ratio from the heavy-ion reactions is from central collisions.

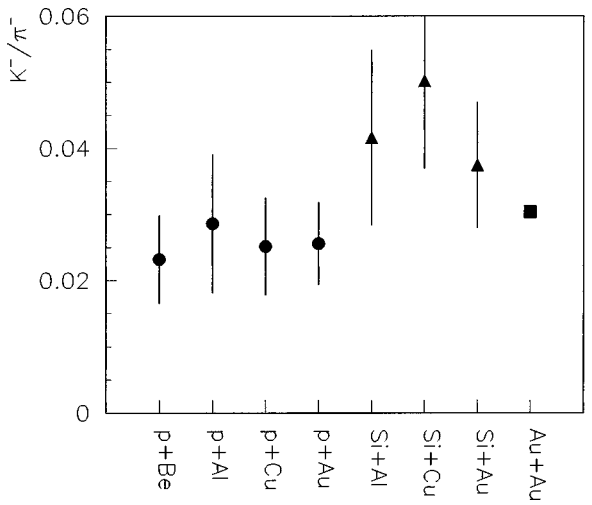

FIG. 26. The K^-/π^- ratio for different beam target combinations. The Au+Au (11.6*A* GeV/*c*) datum is from this paper. The $p+A$(14.6 GeV/*c*) and Si+*A*(14.6*A* GeV/*c*) points are from Refs. [7] and [8], respectively. Each ratio from the heavy-ion reactions is from central collisions.

0.026 ± 0.006, respectively. These results are summarized in Fig. 26, where the K^-/π^- ratio is plotted for each beam and target combination. Note that the K^-/π^- ratio decreases by 30% in $p+p$ reactions from the Si beam energy to the Au beam energy. Given the size of the uncertainty in the proton and Si data, and the difference in beam energies, it is difficult to deduce a trend in this ratio with system size.

VI. CONCLUSIONS

In this paper, the systematics of measured K^+ and K^- spectra in Au+Au reactions at 11.6*A* GeV/*c* have been reported. The measured invariant yields of kaons are well described by exponentials in m_t. The inverse slope parameters *T* are largest at midrapidity and increase with centrality. The inverse slopes increase from 150 MeV in peripheral collisions to 200–220 MeV in central collisions near midrapidity. The centrality dependence of the slope parameters is consistent with more multiscattering occurring in central reactions, extending the spectra out to larger m_t and increasing the inverse slope. The spectra for K^+ are slightly harder than the K^- spectra, i.e., $T_{K^+} > T_{K^-}$ by about 10 to 20 MeV, possibly because there is less phase space available for K^- production. Near midrapidity for central collisions, the m_t spectral shapes for K^+ and K^- are similar.

The rapidity distributions for both K^+ and K^- peak at midrapidity and are approximately Gaussian. The fitted width of the $K^- dN/dy$ distributions σ_{K^-} ranges from 0.72 to 0.76 units of rapidity. The widths are narrower than those from the K^+ distributions ($\sigma_{K^+} = 0.86$–0.99). The difference between the widths is observed in all centrality classes and in $p+p$ reactions. Since the yields of kaons in central reactions are dominated by secondary collisions, these secondary collisions maintain the wider rapidity width of K^+ production observed in $p+p$ kaon production.

The yields of K^+ and K^- increase nonlinearly and steadily with the number of projectile participants. There is no indication of an additional onset of extra kaon production in the most central collisions. The total yields of K^+ and K^- in central Au+Au collisions are 24.2 ± 0.9 and 4.14 ± 0.09, respectively.

The yield per projectile participant is 0.137 for K^+ and 0.023 for K^- in the most central collisions. These values are 3.7 ± 0.5 and 2.5 ± 0.4 times larger than the K^+ and K^- yields from the isospin-averaged *N*-*N* collisions at the same beam energy, respectively. This extra production most probably comes from multiple secondary collisions of hadrons in a heavy-ion reaction [4–6].

The yields of K^- and K^+ increase similarly with centrality. The K^-/K^+ ratio is about 0.17 and is constant over the range of measured centrality, but below the value from *N*-*N* collisions at the same beam energy. Given the many differences between K^- and K^+ production, absorption, the observation that the K^-/K^+ ratio is constant with centrality is a puzzle.

The ratio of fiducial yields from central Au+Au reactions of $K^+/\pi^+ = 0.197 \pm 0.003 \pm 0.010$ continues the steady increase observed from $p+A$ and Si+*A* reactions. The ratio of fiducial yields from central reactions $K^-/\pi^- = 0.0304 \pm 0.0004 \pm 0.0015$ is at the same level or lower than the statistically less accurate Si+*A* results. It is possible that K^- production is more sensitive to the lower beam energy of the Au reactions (11.6*A* GeV/*c*) compared to Si reactions (14.6*A* GeV/*c*).

The systematics of the spectra and yields of K^+ and K^- versus centrality have indicated the importance of multiple collisions and different production thresholds for K^- and K^+. The data can be used to confront the hadronic models that attempt to describe heavy-ion reactions. Each of these models treats the multiple collisions of hadrons in a different manner. These data can be used to test and differentiate between these models.

There are predictions [11] that the possible in-medium properties of K^+ and K^- could shift the spectra so that $T_{K^+} > T_{K^-}$ [15,12]. This could be strongest for central data and at midrapidity where the baryon-density is likely to be large. This is not observed in the data, potentially placing a constraint on the role of kaon mean fields in heavy-ion collisions [15,12].

The fact that the transverse spectra and rapidity distributions for K^+ and K^- are different in Au+Au reactions rules out global-equilibrium thermal models that assume common conditions over the whole system and complete kinetic equilibrium. It may, however, be possible to reconcile these data with a modified thermal model, either with a rapidity-dependent chemical potential or temperature, or possibly different freezeout conditions for K^- and K^+.

Hadronic cascade models predict that a small region of very dense nuclear matter is formed during an Au+Au collision. There is no evidence for any onset of new behavior of kaon production as the centrality is changed. There are two possibilities: (1) a baryon-rich QGP is not formed or is very small, (2) the information from such a plasma is lost after hadronization by the many hadronic collisions. The second possibility makes it difficult to set a quantitative limit on QGP formation.

The experimental data on K^+ and K^- presented in this paper help provide the essential systematics necessary for an understanding of heavy-ion reactions at AGS energies. More

quantitatively, the data provide a foundation for detailed comparison with the complicated dynamical models required to interpret these reactions theoretically.

ACKNOWLEDGMENTS

This work was supported by the U.S. Department of Energy under contracts with BNL (No. DE-AC02-98CH10886), Columbia University (No. DE-FG02-86-ER40281), LLNL (No. W-7405-ENG-48), MIT (No. DE-AC02-76ER03069), UC Riverside (No. DE-FG03-86ER40271), by NASA (No. NGR-05-003-513), under contract with the University of California, by Ministry of Education and KOSEF (No. 951-0202-032-2) in Korea, and by the Ministry of Education, Science and Culture of Japan.

APPENDIX

To provide a baseline for kaon production in Au+Au collisions, it is useful to know the yield of kaons from $p+p$, $p+n$, and $n+n$ collisions at the same beam energy. These can be weighted by the number of collisions between nucleons to provide the average yield of kaons from initial $N+N$ collisions in a Au+Au reaction.

The cross sections for $p+n$ and $n+n$ reactions have not been measured, but can be estimated using isospin symmetry [30]. As an example, K^+ and K^0 form an isospin doublet. There are six cross sections $\sigma_{N+N\rightarrow K+X}$ for the combinations $N=n,p$ and $K=K^0,K^+$.

From isospin symmetry there are three constraints:

$$\sigma_{p+p\rightarrow K^+ +X}=\sigma_{n+n\rightarrow K^0+X}, \tag{A1}$$

$$\sigma_{p+p\rightarrow K^0+X}=\sigma_{n+n\rightarrow K^+ +X}, \tag{A2}$$

$$\sigma_{p+n\rightarrow K^+ +X}=\sigma_{p+n\rightarrow K^0+X}. \tag{A3}$$

TABLE V. The $p+p$ cross sections [20,21] used to calculate the $n+n$, $p+n$, and isospin averaged cross sections. A systematic error of 10% is included in the $N+N$ cross sections.

	$p+p\sigma$ (mb)	$n+p\sigma$ (mb) deduced	$n+n\sigma$ (mb) deduced	$N+N\sigma$ (mb) weighted average
K^+	1.430 ± 0.049	1.16 ± 0.06	0.88 ± 0.06	$1.10\pm0.04\pm0.11$
K^-	0.226 ± 0.023	0.27 ± 0.05	0.32 ± 0.04	$0.28\pm0.02\pm0.02$
K_s^0	0.600 ± 0.012			
Y	1.77 ± 0.06			
$\overline{Y}$	0.003 ± 0.002			
K^0	0.88 ± 0.04			
$\overline{K^0}$	0.32 ± 0.04			

The same assumption as Ref. [30] is made:

$$\sigma_{p+n\rightarrow K^+ +X}=0.5\times(\sigma_{p+p\rightarrow K^+ +X}+\sigma_{n+n\rightarrow K^+ +X}). \tag{A4}$$

With six cross sections and four constraints, the system is fully determined if two of the cross sections are known. The cross section $\sigma_{p+p\rightarrow K^+ +X}$ has been measured at 12 GeV/c [28] and the cross section $\sigma_{p+p\rightarrow K^0+X}$ can be deduced [30] from the measured [29] $\sigma_{p+p\rightarrow K_S^0+X}$ and $\sigma_{p+p\rightarrow Y+X}$ cross sections. The same algorithm is used for the isospin doublet $K^-,\overline{K^0}$.

Table V lists the $p+p$, $p+n$, $n+n$, and isospin-averaged $N+N$ cross sections used in this paper. A systematic error of 10% is assigned to the $N+N$ cross sections. This includes the systematic uncertainty of the $p+p$ experiments and the assumptions used to derive the isospin-averaged cross sections.

[1] *Proceedings of Quark Matter '96* [Nucl. Phys. **A610** (1996)].
[2] G. E. Brown *et al.*, Nucl. Phys. **A567**, 937 (1994).
[3] T. Abbott *et al.*, Phys. Rev. Lett. **64**, 847 (1990); O. Hansen, Comments Nucl. Part. Phys. **20**, 1 (1991).
[4] H. Sorge, H. Stöcker, and W. Greiner, Ann. Phys. (N.Y.) **192**, 266 (1989).
[5] Y. Pang, T. J. Schlagel, and S. H. Kahana, Phys. Rev. Lett. **68**, 2743 (1992).
[6] B-A. Li and C. M. Ko, Phys. Rev. C **52**, 2037 (1995).
[7] T. Abbott *et al.*, Phys. Rev. D **45**, 3906 (1992).
[8] T. Abbott *et al.*, Phys. Lett. B **291**, 341 (1991); T. Abbott *et al.*, Phys. Rev. C **50**, 1024 (1994).
[9] L. Ahle *et al.*, E866 Collaboration, Phys. Rev. C **57**, R466 (1998); L. Ahle *et al.*, Nucl. Phys. **A610**, 139c (1996).
[10] J. Rafelski and B. Müller, Phys. Rev. Lett. **48**, 1066 (1982).
[11] W. Weise, Nucl. Phys. **A610**, 35c (1996).
[12] B.-A. Li and C. M. Ko, Phys. Rev. C **54**, 3283 (1996).
[13] W. Ehehalt and W. Cassing, Nucl. Phys. **A602**, 449 (1996).
[14] E. Friedman, A. Gal, and C. J. Batty, Nucl. Phys. **A579**, 518 (1994).
[15] X. S. Fang *et al.*, Phys. Rev. C **47**, 1678 (1993).
[16] T. Abbott *et al.*, Nucl. Instrum. Methods Phys. Res. A **290**, 41 (1990).
[17] R. Debbe *et al.*, Nucl. Instrum. Methods Phys. Res. A **403**, 256 (1998).
[18] W. A. Zajc, *4th Conference on the Intersections between Particle and Nuclear Physics*, AIP Conf. Proc. 243, edited by W. T. H. Van Oers (AIP, New York, 1991); V. Cianciolo, Ph.D. thesis, MIT, 1994.
[19] T. Abbott *et al.*, E802 Collaboration, Phys. Rev. C **44**, 1611 (1991).
[20] GEANT 3.2.1, CERN Program Library W5013, 1993 (unpublished).
[21] Particle Data Group, R. M. Barnett *et al.*, Phys. Rev. D **54**, 11 (1996).
[22] A. M. Rossi *et al.*, Nucl. Phys. **B84**, 269 (1975).
[23] Rossi *et al.* [22] reported the $\langle p_t\rangle$ for K^+ and K^- from $p+p$ reactions integrated over rapidity space to be 414 and 392 MeV/c, respectively. The relative uncertainty is quoted as a few percent. The inverse slope parameters of an exponen-

tial m_t spectrum that reproduces these mean $\langle p_t \rangle$ values are $T=143$, $T=132$ MeV for K^+ and K^-, respectively.
[24] S. Chapman and J. R. Nix, Phys. Rev. C **54**, 866 (1996).
[25] E. Schnedermann, J. Sollfrank, and U. Heinz, Phys. Rev. C **48**, 2462 (1993).
[26] P. Braun-Munzinger *et al.*, Phys. Lett. B **344**, 43 (1995).
[27] J. Cleymans *et al.*, Z. Phys. C **74**, 319 (1997).
[28] H. Fesefeldt *et al.*, Nucl. Phys. **B147**, 317 (1979).
[29] V. Blobel *et al.*, Nucl. Phys. **B69**, 454 (1974).
[30] M. Gazdzicki and O. Hansen, Nucl. Phys. **A528**, 754 (1991).